LASER & PHOTONICS REVIEWS

www.lpr-journal.org

Femtosecond Frequency Combs with Few-kHz Passive Stability over an Ultrabroadband Spectral Range

*Sarah R. Hutter, Ali Seer, Tilman König, Robert Herda, Daniel Hertzsch, Hannes Kempf, Rafal Wilk, and Alfred Leitenstorfer**

Femtosecond frequency combs are among the most precise measurement tools in existence. They have applications ranging from high-precision spectroscopy and metrology to time-domain quantum physics. Maximizing the passive stability of these instruments is essential to achieve their full potential in fundamental science and high-tech industry. However, the noise mechanisms across the entire operating space of these devices have not been fully characterized. Here the noise properties of fiber-based frequency combs are studied as a function of intracavity dispersion, pump power, and repetition rate. Distinct minima are discovered in this parameter space where the free-running linewidth of the carrier-envelope offset (CEO) frequency f_{CEO} drops below 1 kHz. The individual comb lines are analyzed spread over a wide spectral range producing a complete understanding of the particular contributions to the phase noise and their interplay. Exploiting these findings, combs featuring sharp teeth at specific frequency positions and over the entire spectrum from f_{CEO} to 300 THz are demonstrated. The ultrabroadband stability offered by these compact systems provides a new level of quality for front-end measurement tasks in both time and frequency domains.

1. Introduction

Optical frequency combs (OFCs)[1,2] based on mode-locked lasers consist of a spectrum of equidistant lines, so-called comb teeth, separated by the repetition rate f_r of the cavity. The entire comb is shifted from the origin by the carrier-envelope offset frequency f_{CEO}. Consequently, the spectral position of every tooth is defined by its mode number n and two characteristic radio frequencies (RF): $\nu_n = f_{CEO} + nf_r$.[3–5] Since both f_r and f_{CEO} may be determined precisely by electronic counting, OFCs provide a unique link between the RF and optical domains.[6] Today, such systems are typically based on optical fiber technology[7,8] offering favorable compactness, stability, and low power consumption.[9,10]

The phase noise properties of frequency combs determine their performance in various applications[7,8,11,12] such as optical atomic clocks[13] and ultraprecision spectroscopy.[14,15] Thus, OFCs with extremely narrow linewidths are in high demand. Theoretical studies discussing the noise in mode-locked lasers[16–18] predict that minimizing the cavity dispersion reduces the phase noise of f_r, the so-called timing jitter. This finding has been verified by several groups.[19–21] However, previous studies have analyzed the impact of cavity dispersion on one specific frequency region within a comb, respectively. In contrast, we quantify and model the noise performance of several spectral parts of the comb which are distributed over an ultrabroadband range. Our results are fully consistent with the elastic tape picture[22,23] which allows us to apply our insights to tailor-design various ultraprecise oscillators optimized for specific measurement tasks in the time and frequency domains. We advance free-running fiber combs into the regime of sub-kHz linewidths and achieve few-kHz performance over the entire range from the CEO frequency to the shortwave end of optical emission.

2. Results and Discussion

2.1. Experimental Setup

Our experiment is sketched in **Figure 1**. A femtosecond Er:fiber oscillator based on additive-pulse mode-locking[24–26] is the core. It consists of a nonlinear amplifying loop mirror (NALM)[27–29] with a short free-space part. This compact design allows repetition rates up to 250 MHz. Adjustable polarization optics (PO) in the linear section of the laser enable sensitive alignment of the non-reciprocal phase bias. This off-resonant modelocking scheme does not add any significant dispersion. Polarization-maintaining optical fibers minimize environmental

S. R. Hutter, T. König, D. Hertzsch, H. Kempf, A. Leitenstorfer
Department of Physics and Center for Applied Photonics
University of Konstanz
78457 Konstanz, Germany
E-mail: aleitens@uni-konstanz.de

A. Seer, R. Herda, R. Wilk
Toptica Photonics AG
Lochhamer Schlag 19, 82166 Gräfelfing, Germany

The ORCID identification number(s) for the author(s) of this article can be found under https://doi.org/10.1002/lpor.202200907

DOI: 10.1002/lpor.202200907

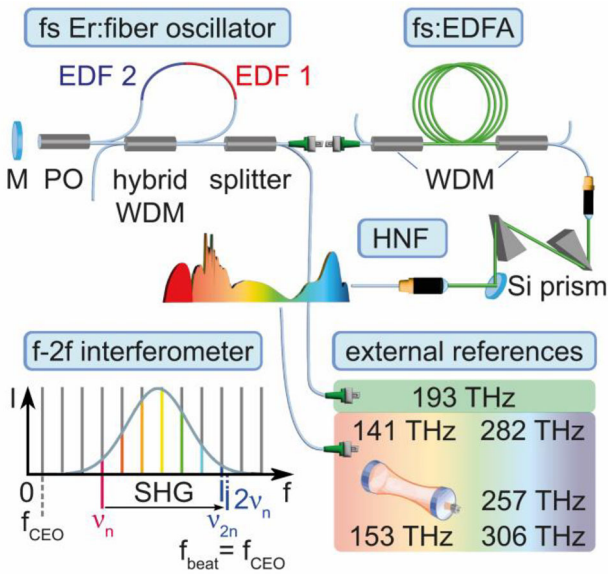

Figure 1. Schematic overview of mode-locked Er:fiber system and setup for ultrabroadband characterization of phase noise. The gain medium of the oscillator is composed of two different Er-doped fibers (EDF1, EDF2). PO: polarization optics; WDM: wavelength division multiplexer; M: mirror. The pulse train passes a femtosecond Er:fiber amplifier (fs:EDFA) and a silicon (Si) prism sequence. Subsequently, a highly nonlinear fiber (HNF) generates a supercontinuum, enabling f-2f interferometry. Frequencies of single-line optical references and their subharmonics are listed in the bottom right corner.

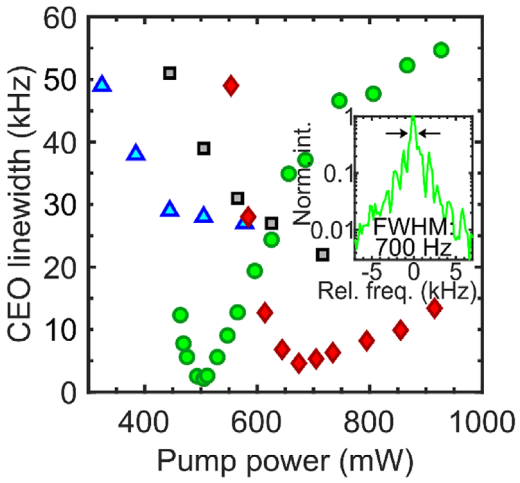

Figure 2. CEO linewidth versus pump power P of four oscillators differing in cavity dispersion only. $\beta_{2,cav} = -830$ fs^2 (black squares), -130 fs^2 (blue triangles), $+1100$ fs^2 (green circles), and $+1300$ fs^2 (red diamonds). Each data point represents the average value of 10 measurements. Error bars are not shown as standard deviations are smaller than marker size. The inset highlights the frequency spectrum of the CEO beat at $\beta_{2,cav} = +1100$ fs^2 and P = 505 mW (18.9 ms sweep time, 50 kHz measurement span, 200 Hz resolution bandwidth, 30 Hz video bandwidth). All data depicted here were taken in stable single-pulse operation of the laser cavity.

disturbances. Two different erbium-doped fibers form the gain medium: the second-order dispersion β_2 of EDF1 is normal with +49 200 fs^2 m^{-1} whereas EDF2 exhibits anomalous dispersion ($\beta_2 = -22100$ fs^2 m^{-1}). By adjusting the ratio between both EDFs without changing the length of the gain section, we may vary the intracavity dispersion $\beta_{2,cav}$ while all other laser parameters stay identical.

The oscillator is followed by a single-pass Er:fiber amplifier (fs:EDFA)[30] boosting the output pulses to several nJ. Subsequently, a highly nonlinear fiber (HNF)[30] generates a supercontinuum spanning from 135 to 370 THz, that efficiently supports f-2f interferometry.[4,5] Beating the second harmonic (SHG) of the nth comb line with the (2n)th mode provides the carrier-envelope offset frequency f_{CEO}:

$$f_{CEO} = 2\nu_n - \nu_{2n} \tag{1}$$

The beat note is recorded with a RF spectrum analyzer and its full width at half maximum (FWHM) is investigated.

2.2. CEO and Optical Linewidths: Influence of Cavity Dispersion and Pump Power

We investigate the performance of a 200-MHz comb by systematically changing its intracavity dispersion in nine steps between -3000 fs^2 and $+2000$ fs^2. The CEO linewidth δ_{CEO} of four typical examples is presented in **Figure 2** as a function of the pump power P. Interestingly, the normally dispersive oscillators (green dots: $\beta_{2,cav} = +1100$ fs^2; red diamonds: $\beta_{2,cav} = +1300$ fs^2) exhibit distinct minima while the linewidth of those with anomalous cavity dispersion changes monotonously (black squares: $\beta_{2,cav} = -830$ fs^2; blue triangles: $\beta_{2,cav} = -130$ fs^2). The most extreme case occurs at $+1100$ fs^2 (green) where δ_{CEO} drops to 700 Hz (FWHM) at $P = 505$ mW (see inset in Figure 2). According to our knowledge, this is the smallest free-running CEO linewidth ever recorded for a fiber laser. Until now, sub-kHz passive performance was reached only with a monolithic solid-state laser.[31]

To draw maximum benefits from the observation above, we develop a profound understanding of the phenomenon. To this end, a broadband analysis of the frequency noise $\Delta\nu(f)$ of the oscillator with $\beta_{2,cav} = +1100$ fs^2 is carried out. We investigate $\Delta\nu(f)$ of f_{CEO} via f-2f interferometry. Three selected comb lines in the optical range between 141 and 282 THz are characterized by beating them with narrowband external references (lower right in Figure 1). The recorded time traces (400 ms observation time) are analyzed with a Takeda algorithm[32] and the frequency noise spectral density $S_{\Delta\nu}(f)$ is computed. **Figure 3**a illustrates $S_{\Delta\nu}(f)$ for f_{CEO} (green), 141 THz (orange), 193 THz (cyan), and 282 THz (black) at $P = 505$ mW. The frequency noise of f_{CEO} is essentially white, pointing at a quantum process dominated by amplified spontaneous emission (ASE).[16,33] In contrast, the noise spectra of the optical lines are more complex. We analyze the additional contributions based on the spectrum recorded at 282 THz (black graph in Figure 3b). A low-pass characteristic is found at kHz frequencies, which originates from intensity fluctuations of the pump.[34]

The noise spectral density is given by

$$S_{\Delta\nu}(f) = \frac{S_{\Delta\nu}(0)}{1 + \left(f/f_{3dB}\right)^2} \tag{2}$$

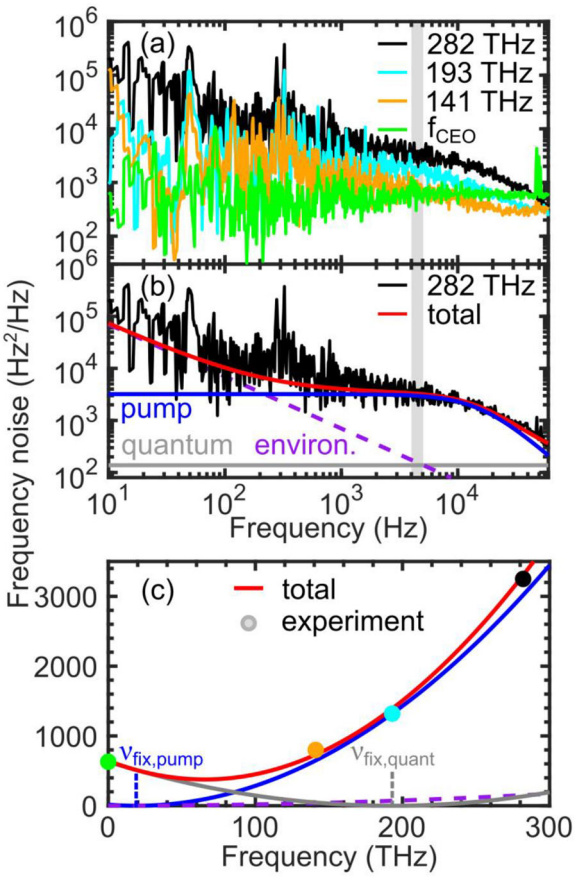

Figure 3. Broadband frequency noise analysis of oscillator with $\beta_{2,cav} = +1100\ \mathrm{fs}^2$ at $P = 505$ mW. a) Frequency noise spectral density at f_{CEO} (green) and for comb lines at 141 THz (2120 nm, orange), 193 THz (1550 nm, cyan), and 282 THz (1060 nm, black). b) Spectral characteristics of quantum (gray), environmental (purple dashed), and pump noise (blue) contributing to the total (red) noise spectral density of the mode at 282 THz. c) Noise level between 4 and 5 kHz (gray marker in (a)) of the individual comb teeth (dots with color coding as in (a)). All three contributions are significant in this band. Gray, blue and purple dashed parabolas: quantum, pump, and environmental noise with fixed points at 193 THz, 19 THz, and 0 THz, respectively. Red graph: sum of all components.

where f_{3dB} is the 3 dB roll-off frequency of the oscillator response determined by the characteristic timescales for gain and losses.[35] For frequencies below 1 kHz, a component decreasing with $1/f$ emerges. We attribute this feature to environmental noise such as acoustic or thermal disturbances, affecting mostly the cavity length.[34,36] By fitting the sum (red) of a flat spectrum for the quantum contribution (gray), a low-pass characteristics with $f_{3dB} = 16$ kHz for the pump noise (blue) and a $1/f$ component due to environmental influences (purple dashed), we recover the total noise spectrum at 282 THz (black).

Next, we study the spectral dependence of the individual components. Qualitative access to the phase noise correlations between the longitudinal modes is provided by the elastic tape picture.[22,23] This model visualizes the comb teeth on a rubber band stretching and contracting due to fluctuations in f_r while translating sideways upon changing f_{CEO}. For each noise component, a fixed point ν_{fix} is not affected by this breathing motion. Away from ν_{fix}, the noise level increases quadratically.[37] For ASE-induced phase fluctuations, $\nu_{fix,quant}$ coincides with the optical carrier frequency ν_c.[34,38] The dots in Figure 3c are color-coded according to Figure 3a and represent the average value of the frequency noise in the RF band between 4 and 5 kHz (see vertical gray bar in (a) and (b)). As the phase noise is quantum-limited at f_{CEO} (green dot), we can directly determine the level of quantum noise as a function of optical frequency. The resulting parabola with a minimum at $\nu_{fix,quant} = 193$ THz is plotted in gray. Extracting the level of pump noise at the optical comb lines from the fitted low-pass characteristics and adapting a parabolic function (blue) reveals that the fixed point of the pump noise $\nu_{fix,pump}$ resides at 19 THz. Environmental noise leading to fluctuations of the cavity length features a fixed point at 0 THz. This fact determines the minimum of the purple-dashed parabola and the value extracted from the 1/f fit at 282 THz (purple dashed line in Figure 3b) the curvature. The sum of all three contributions (red) is in excellent agreement with our measurement. We emphasize that any comb teeth below 80 THz are quantum-limited in this configuration.

2.3. Pump-Induced Phase Noise

The location of $\nu_{fix,pump}$ determines which comb lines are not broadened by pump noise. The ability to precisely select this spectral band will establish a new generation of tailor-designed OFCs with ultralow noise. Toward this goal, we first investigate the dependence of $\nu_{fix,pump}$ on P. The results of an analysis analogous to Figure 3 are depicted as green circles in **Figure 4**a. Interestingly, $\nu_{fix,pump}$ varies over a range of 300 THz while the oscillator maintains stable one-pulse operation. Note that the negative fixed-point frequencies for $P < 500$ mW correspond to a correlated movement of all comb lines without one being locked into position. In theory, the fixed point is given by[34,35]

$$\nu_{fix,pump} = \nu_c + f_r^2 \frac{d\varphi/dP}{df_r/dP} \tag{3}$$

Here, ν_c and φ are the carrier frequency and phase (in radian). First, we discuss the denominator of Equation (3). Variations in pump power influence the repetition rate in three ways:[35,39]

$$\frac{df_r}{dP} = -f_r^2 \left(\underbrace{\beta_{2,cav} \frac{d\omega_c}{dP}}_{\text{spec.shift}} + \underbrace{\frac{\gamma}{\omega_c} \frac{dA^2}{dP}}_{\text{self-steep.}} + \underbrace{\frac{1}{\Omega_g} \frac{dg}{dP}}_{\text{res.gain}} \right) \tag{4}$$

The first term in Equation (4) considers the spectral shift of the center frequency ω_c. Since this contribution scales with $\beta_{2,cav}$, df_r/dP becomes large far away from zero dispersion and Equation (3) may be simplified as $\nu_{fix,pump} \approx \nu_c$. The second term indicates a pump-induced change in f_r due to self-steepening. It depends on the peak intensity A^2 and the total nonlinearity $\gamma = 1.5\ \mathrm{kW}^{-1}$ determined by the fiber length in the resonator. Additionally, a change in P varies the gain g. This resonant gain contribution is inversely proportional to the width of the optical gain spectrum $\Omega_g = 3\ \mathrm{THz} \times 2\pi$. The derivative dg/dP may be

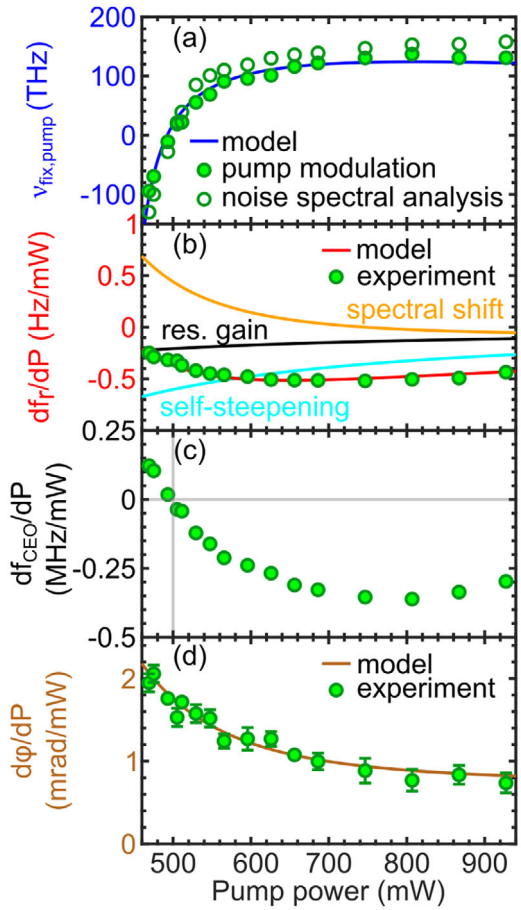

Figure 4. Impact of pump stability on frequency comb parameters versus pump power. a) Fixed points deduced from noise spectral analysis (green circles), by pump modulation (green dots) and modeling (blue line). b) Pump-induced changes of repetition rate (green dots). The model (red) includes contributions from spectral shifts (orange), resonant gain (black), and self-steepening effects (cyan). c) Sensitivity of CEO frequency to pump power fluctuations. a–c): Error bars are not shown as standard deviations are smaller than marker size. d) Green dots: pump power gradient of carrier phase extracted from data in (b) and (c). Error bars are obtained via propagation of uncertainties. Brown line: theory.

approximated[35] as $f_{3dB}^{Er}/(f_{3dB}2P)$ where we adopt a reaction bandwidth f_{3dB}^{Er} of the Er:gain section of 1.6 kHz.[35] Altogether, we may calculate the pump-induced change in repetition rate df_r/dP by analyzing the output spectrum and power of the oscillator. Figure 4b displays the pump power dependence of the individual contributions to Equation (4) and their sum (red).

We directly measure df_r/dP by slightly modulating P with a square wave and recording f_r with a high-resolution frequency counter (1 ms gate time). The results (green dots in Figure 4b) are represented excellently by the model based on Equation (4). Next, we monitor f_{CEO} with the same method (Figure 4c). From this analysis, we understand that the distinct minimum of CEO linewidth (Figure 2) emerges because f_{CEO} is inert against pump power fluctuations (horizontal gray line) at $P = 500$ mW (vertical gray line). Generally, a pump-induced change in f_{CEO} results from variations of both the repetition rate f_r and the carrier phase φ:[35,39]

$$\frac{df_{CEO}}{dP} = \frac{v_c}{f_r}\frac{df_r}{dP} + f_r\frac{d\varphi}{dP} \tag{5}$$

By inverting this equation and adopting the experimental values for df_r/dP and df_{CEO}/dP (Figure 4b,c), we obtain $d\varphi/dP$ (numerator in Equation (3)). The results and computed phase changes of a soliton with respect to pump fluctuations[39]

$$\frac{d\varphi}{dP} = \frac{\gamma}{4\pi}\frac{dA^2}{dP} \tag{6}$$

are depicted as green dots and brown line in Figure 4d. We now calculate $\nu_{fix,pump}$ as a function of P based on Equations (3), (4), and (6) (blue line in Figure 4a). Alternatively, the fixed point may be determined by inserting the data for df_r/dP and $d\varphi/dP$ gained through pump power modulation (Figure 4b,d) into Equation (3). The consistency of this straightforward approach (green dots) with noise spectral analysis (green circles) and our model (blue) is impressively evidenced by Figure 4a.

2.4. Designing Ultraprecise Frequency Combs

Having understood the effects determining $\nu_{fix,pump}$, we may now select its location. Since this spectral region features the comb lines which are not broadened by pump noise, it should coincide with the frequency range targeted by the future application of the OFC. To design an oscillator optimized for subsequent generation of, e.g., an ultrastable dispersive wave covering frequencies between 200 and 350 THz,[30] $\nu_{fix,pump}$ should be located in the center of this band, i.e., significantly above $\nu_c = 193$ THz. To this end, an increase in pump power has to result in an acceleration of the pulse envelope ($df_r/dP > 0$), as $d\varphi/dP$ is always positive (see Equations (3) and (6)). Therefore, a spectral blue shift has to occur in case of anomalous intracavity dispersion. Additionally, this mechanism must be strong enough to compensate for the two other contributions in Equation (4) which are always negative.

The output spectra of an 83-MHz oscillator ($\beta_{2,cav} = -1300$ fs^2, $\gamma = 4.1$ kW^{-1}) are color-coded versus pump power in **Figure 5**a. For $P < 210$ mW, increasing the pump power shifts the pulse toward higher center frequencies. Figure 5b illustrates df_r/dP due to this spectral shift (orange line), the resonant gain (black) and self-steepening (cyan) according to Equation (4). The sum of all contributions (red) is positive for 140 mW $\leq P \leq$ 170 mW (highlighted by dashed line and red area). We now insert these theoretical values and the calculated phase changes (Equation (6)) in Equation (3) to compute $\nu_{fix,pump}$ as a function of P. Figure 5c demonstrates that our model (red) coincides excellently with experimental data obtained from noise spectral analysis (yellow diamonds). We emphasize that $\nu_{fix,pump}$ is above ν_c for 140 mW $\leq P \leq$ 170 mW and may be varied between −150 and 400 THz during stable single-pulse operation.

Tailoring $\nu_{fix,pump}$ is essential for designing ultralow-noise OFCs. Moreover, we achieve sharp teeth in a broad spectral range by minimizing the curvature of the quadratic increase in phase noise away from the fixed points. Generally, the frequency noise

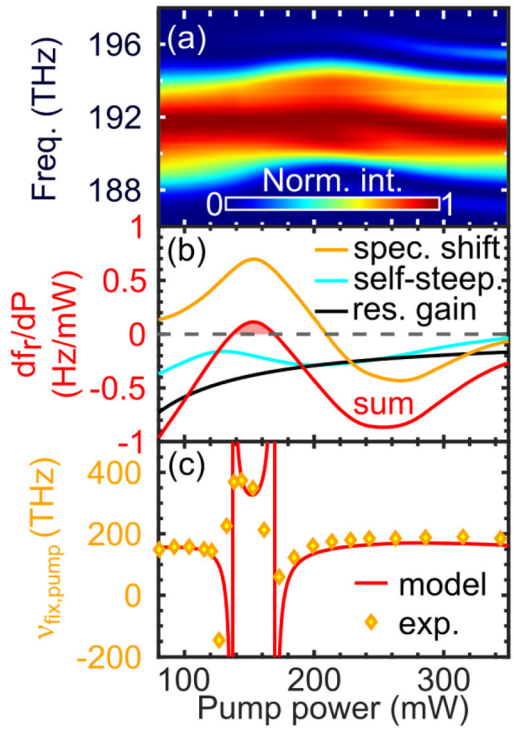

Figure 5. Characteristics of an 83-MHz oscillator versus pump power. a) Color-coded output spectra. b) Calculated changes of the repetition rate. Yellow line: spectral shift, cyan: self-steepening, black: resonant gain, red: sum. c) Fixed-point frequencies extracted from noise spectral analysis (yellow diamonds) and modeling (red).

spectral density $S_{\Delta\nu}(f)$ of a comb tooth at frequency ν is given by:[37]

$$S_{\Delta\nu,\nu}(f) = f_r^{-2}\left[S_{rep}^{quant}(\nu-\nu_c)^2 + S_{rep}^{env}(f)(\nu)^2 + S_{rep}^{pump}(f)(\nu-\nu_{fix,pump})^2\right] \quad (7)$$

Developing oscillators close to zero dispersion featuring high circulating powers and spectrally broad pulses keeps ASE-induced fluctuations of the repetition rate S_{rep}^{quant} to a minimum.[34] The influence of environmental noise is reduced by shielding the cavity. When both contributions are minimized as in our case, pump-induced fluctuations of the repetition rate S_{rep}^{pump} dominate. Their noise spectral density may be expressed as[34]

$$S_{rep}^{pump}(f) = S_{RIN}P^2\left(\frac{df_r}{dP}\right)^2\frac{1}{1+(f/f_{3dB})^2} \quad (8)$$

S_{RIN} denotes the relative intensity noise of the pump laser which is minimized by state-of-the-art diodes operated at high currents.[37,40] A low-loss cavity with highly efficient fiber components keeps P moderate. Thus, key for low-noise operation is to minimize df_r/dP (Equation (4)). Therefore, we aim at compensating the impacts of resonant gain and self-steepening by adjusting the effect of spectral shift via the cavity dispersion. Measuring df_r/dP together with the output spectrum determines whether

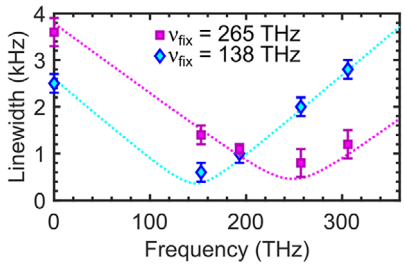

Figure 6. Tailor-designed ultralow-noise 40-MHz oscillators. Linewidths of comb with $\nu_{fix,pump}$ = 265 THz (1128 nm, magenta squares) and of comb with $\nu_{fix,pump}$ = 138 THz (2167 nm, blue diamonds) versus frequency. Data points represent the average of 10 individual measurements, each taken for 123 ms. Error bars indicate standard deviations. Purple and blue dotted lines represent the linewidths calculated from the model, respectively.

$\beta_{2,cav}$ needs to be increased or decreased. This fine-tuning is done by slightly adjusting the fiber lengths. From Equation (8), the flattest curvature of the quadratic increase in pump-induced frequency noise is gained by minimizing df_r/dP. At the same time, the precise value of df_r/dP sets the position of $\nu_{fix,pump}$ (Equation (3)) and the region with narrowest linewidths.

Iterating in this way, we design two ultralow-noise 40-MHz oscillators optimized for specific examples of tasks in precision metrology. The first comb with $\beta_{2,cav}$ = +2800 fs^2 and γ = 10.9 kW^{-1} features $\nu_{fix,pump}$ = 138 THz at P = 38 mW. Owing to its fixed point in the short-wavelength mid infrared, it is perfectly suited, e.g., for applications of ultrafast spectroscopy in this spectral band where minute amplitude or phase changes due to excitation of a sample are to be determined. For P = 38 mW, we measure df_r/dP = −0.14 Hz mW^{-1}. Such low values of df_r/dP and P are promising ultranarrow linewidths over a wide range. The spectral purity of the single-line references used so far is insufficient for characterizing this comb. Therefore, we now harness the stability of a high-finesse ultralow expansion cavity with a linewidth <1.5 Hz (1s measurement time).[41] The reference frequencies available are summarized at the bottom right in Figure 1. The FWHM of the corresponding beat signals and the CEO linewidth are depicted as blue diamonds in **Figure 6**. Note that this OFC features teeth with linewidths below 3 kHz in an ultrabroadband range covering more than 300 THz with an absolute minimum of 600 Hz at 153 THz.

The second oscillator ($\beta_{2,cav}$ = +3100 fs^2 and γ = 11.3 kW^{-1}) is tailor-designed for applications in time-domain quantum physics. With $\nu_{fix,pump}$ = 265 THz and df_r/dP = +0.15 Hz mW^{-1} at P = 30 mW, it features sub-kHz linewidths between 200 THz and 300 THz (purple squares and dotted line in Figure 6). Hence, this frequency comb is ideal for the generation of a broadband dispersive wave centered around 250 THz.[30] These ultrastable few-femtosecond pulses allow very sensitive time-domain sampling of the electric field of mid-infrared states of light and their quantum fluctuations.[42,43] Note that the passive frequency stability of both systems is below 10^{-11} over a measurement time of 123 ms and in the entire optical range covered. To the best of our knowledge, such broadband frequency stability has not been demonstrated previously with any kind of OFC.

Finally, we compare these results with our model including quantum and pump noise. In case of a low-pass characteristics,

the linewidth may be extracted from the frequency noise spectral density by[34]

$$\delta_\nu = \pi \sqrt{S_{\Delta\nu,\nu}(0) f_{3dB}} \tag{9}$$

First, we calculate the pump-induced fluctuations of the repetition rate S_{rep}^{pump} based on Equation (8) and df_r/dP obtained from pump-power modulation. Analyzing the noise spectra of the five comb lines according to Figure 3b,c yields $S_{rep}^{quant} = 6 \times 10^{-12}$ Hz and $f_{3dB} = 1.4$ kHz for both combs. From these inputs, Equations (7) and (9) provide the linewidth as a function of the optical frequency ν. The results are depicted as blue and magenta dotted lines in Figure 6, respectively, and pleasantly agree with experiment.

3. Summary and Outlook

The discovery of distinct minima in CEO linewidth at specific pump powers of mode-locked Er:fiber oscillators has motivated us to systematically analyze the frequency noise of f_{CEO} and various optical comb lines. By varying the intracavity dispersion and repetition rate together with quantitative modeling we produced a complete understanding of the noise performance of femtosecond frequency combs: Owing to extremely low levels of quantum noise, our systems are limited by pump noise. At a particular pumping level, the influence of pump fluctuations on f_{CEO} vanishes, resulting in a quantum-limited linewidth below 1 kHz. We demonstrate that the fixed-point frequency related to pump noise settles to 0 THz at this setpoint. The exact location of $\nu_{fix,pump}$ is tunable via pump power and may be determined by analyzing the spectral noise of at least three comb lines. All findings are matched precisely by a model depending on the dispersion $\beta_{2,cav}$ and nonlinearity γ of the cavity plus variations of the output spectrum and pulse energy with pump power. Based on these insights, we demonstrate a straightforward way to determine $\nu_{fix,pump}$ by simply recording the repetition rate and f_{CEO} upon pump power modulation.

To obtain ultranarrow comb teeth over a broad spectral range, the curvature of the quadratic increase in frequency noise away from $\nu_{fix,pump}$ has to be minimized. Our quantitative understanding enables us to select all parameters such that extremely narrow linewidths emerge simultaneously for one specific pump power. We emphasize that our strategies are applicable to all types of femtosecond frequency combs. Nevertheless, note that taking full advantage of them ideally requires fine tuning of the cavity dispersion over a significant range. The availability of this option may be limited in some types of oscillators that are modelocked, e.g., by resonant means like saturable absorber mirrors. For the case of mode-locked fiber lasers, our insights have allowed us to set the free-running linewidths to the sub-kHz range in a specific frequency band while keeping it below 3 kHz in the entire spectrum from f_{CEO} all the way up to 300 THz. Naturally, such a level of passive noise performance is highly attractive for future advances in precision spectroscopy[14,44] and metrology.[5] While active stabilization may further reduce the linewidth, it requires additional resources and might even enhance the noise at frequencies beyond the locking bandwidth. Consequently, oscillators featuring exquisite free-running stability are mandatory for challenging time-domain applications where modulation is often carried out at radio frequencies. In the near future, they will pave the way, e.g., for strongly enhanced performance in time-domain studies of vacuum fluctuations and squeezed states of terahertz and mid-infrared fields with electro-optic sampling.[42,43,45]

Supporting Information

Supporting Information is available from the Wiley Online Library or from the author.

Acknowledgements

This work was funded by the Deutsche Forschungsgemeinschaft (DFG, German Research Foundation) - SFB 1432 - Project-ID 425217212 and TOPTICA Photonics AG.

Open access funding enabled and organized by Projekt DEAL.

Conflict of Interest

Ali Seer, Robert Herda, and Rafal Wilk are employees of TOPTICA Photonics AG, a company developing high-end laser systems for scientific and industrial applications. The remaining authors declare no competing interests.

Data Availability Statement

The data that support the findings of this study are available from the corresponding author upon reasonable request.

Keywords

femtosecond frequency combs, optical metrology, passive stability, phase noise properties, supercontinuum generation, ultranarrow linewidths

Received: November 24, 2022
Revised: April 6, 2023
Published online: April 22, 2023

[1] J. L. Hall, *Rev. Mod. Phys.* **2006**, *78*, 1279.
[2] T. W. Hänsch, *Rev. Mod. Phys.* **2006**, *78*, 1297.
[3] H. R. Telle, G. Steinmeyer, A. E. Dunlop, J. Stenger, D. H. Sutter, U. Keller, *Appl. Phys. B: Lasers Opt.* **1999**, *69*, 327.
[4] R. Holzwarth, T. Udem, T. W. Hänsch, J. C. Knight, W. J. Wadsworth, P. S. J. Russell, *Phys. Rev. Lett.* **2000**, *85*, 2264.
[5] D. J. Jones, S. A. Diddams, J. K. Ranka, A. Stentz, R. S. Windeler, J. L. Hall, S. T. Cundiff, *Science* **2000**, *288*, 635.
[6] S. A. Diddams, K. Vahala, T. Udem, *Science* **2020**, *369*, 267.
[7] M. E. Fermann, I. Hartl, *Nat. Photonics* **2013**, *7*, 868.
[8] J. Kim, Y. Song, *Adv. Opt. Photonics* **2016**, *8*, 465.
[9] L. C. Sinclair, I. Coddington, W. C. Swann, G. B. Rieker, A. Hati, K. Iwakuni, N. R. Newbury, *Opt. Express* **2014**, *22*, 6996.
[10] M. Lezius, T. Wilken, C. Deutsch, M. Giunta, O. Mandel, A. Thaller, V. Schkolnik, M. Schiemangk, *Optica* **2016**, *3*, 1381.
[11] T. Fortier, E. Baumann, *Commun. Phys.* **2019**, *2*, 1.
[12] E. D. Caldwell, L. C. Sinclair, N. R. Newbury, J. D. Deschenes, *Nature* **2022**, *610*, 667.

[13] A. D. Ludlow, M. M. Boyd, J. Ye, E. Peik, P. O. Schmid, *Rev. Mod. Phys.* **2015**, *87*, 637.
[14] I. Coddington, N. Newbury, W. Swann, *Optica* **2016**, *3*, 414.
[15] Y. Sugiyama, T. Kashimura, K. Kashimoto, D. Akamatsu, F. L. Hong, *Sci. Rep.* **2023**, https://doi.org/10.1038/s41598-023-29734-2.
[16] H. A. Haus, A. Mecozzi, *IEEE J. Quantum Electron.* **1993**, *29*, 983.
[17] H. A. Haus, *IEEE J. Quantum Electron.* **1997**, *33*, 649.
[18] R. Paschotta, *Appl. Phys. B: Lasers Opt.* **2004**, *79*, 163.
[19] L. Nugent-Glandorf, T. A. Johnson, Y. Kobayashi, S. A. Diddams, *Opt. Lett.* **2011**, *36*, 1578.
[20] Y. Song, C. Kim, K. Jung, H. Kim, J. Kim, *Opt. Express* **2011**, *19*, 14518.
[21] A. S. Mayer, W. Grosinger, J. Fellinger, G. Winkler, L. W. Perner, S. Droste, S. H. Salman, C. Li, C. M. Heyl, I. Hartl, O. H. Heckl, *Opt. Express* **2020**, *28*, 18946.
[22] H. R. Telle, B. Lipphardt, J. Stenger, *Appl. Phys. B: Lasers Opt.* **2002**, *74*, 1.
[23] E. Benkler, H. R. Telle, A. Zach, F. Tauser, *Opt. Express* **2005**, *13*, 5662.
[24] E. P. Ippen, H. A. Haus, L. Y. Liu, *J. Opt. Soc. Am. B* **1989**, *6*, 1736.
[25] H. A. Haus, J. G. Fujimoto, E. P. Ippen, *J. Opt. Soc. Am. B* **1991**, *8*, 2068.
[26] H. A. Haus, K. Tamura, L. E. Nelson, E. P. Ippen, *IEEE J. Quantum Electron.* **1995**, *31*, 591.
[27] M. E. Fermann, F. Haberl, M. Hofer, H. Hochreiter, *Opt. Lett.* **1990**, *15*, 752.
[28] N. Kuse, J. Jiang, C.-C. Lee, T. R. Schibli, M. E. Fermann, *Opt. Express* **2016**, *24*, 3095.
[29] T. Jiang, Y. Cui, P. Lu, C. Li, A. Wang, Z. Zhang, *IEEE Photonics Technol. Lett.* **2016**, *28*, 1786.
[30] D. Brida, G. Krauss, A. Sell, A. Leitenstorfer, *Laser Photonics Rev.* **2014**, *8*, 409.
[31] T. D. Shoji, W. Xie, K. L. Silverman, A. Feldman, T. Harvey, R. P. Mirin, T. R. Schibli, *Optica* **2016**, *3*, 995.
[32] M. Takeda, H. Ina, S. Kobayashi, *J. Opt. Soc. Am.* **1982**, *72*, 156.
[33] R. Paschotta, A. Schlatter, S. C. Zeller, H. R. Telle, U. Keller, *Appl. Phys. B: Lasers Opt.* **2006**, *82*, 265.
[34] N. R. Newbury, W. C. Swann, *J. Opt. Soc. Am. B* **2007**, *24*, 1756.
[35] B. R. Washburn, W. C. Swann, N. R. Newbury, *Opt. Express* **2005**, *13*, 10622.
[36] S. Droste, G. Ycas, B. R. Washburn, I. Coddington, N. R. Newbury, *Nanophotonics* **2016**, *5*, 196.
[37] J. J. McFerran, W. C. Swann, B. R. Washburn, N. R. Newbury, *Opt. Lett.* **2006**, *31*, 1997.
[38] A. Liehl, P. Sulzer, D. Fehrenbacher, T. Rybka, D. V. Seletskiy, A. Leitenstorfer, *Phys. Rev. Lett.* **2019**, *122*, 203902.
[39] N. R. Newbury, B. R. Washburn, *IEEE J. Quantum Electron.* **2005**, *41*, 1388.
[40] J. J. McFerran, W. C. Swann, B. R. Washburn, N. R. Newbury, *Appl. Phys. B: Lasers Opt.* **2007**, *86*, 219.
[41] T. Puppe, A. Sell, R. Kliese, N. Hoghooghi, A. Zach, W. Kaenders, *Opt. Lett.* **2016**, *41*, 1877.
[42] C. Riek, D. V. Seletskiy, A. S. Moskalenko, J. F. Schmidt, P. Krauspe, S. Eckart, S. Eggert, G. Burkard, A. Leitenstorfer, *Science* **2015**, *350*, 420.
[43] C. Riek, P. Sulzer, M. Seeger, A. S. Moskalenko, G. Burkard, D. V. Seletskiy, A. Leitenstorfer, *Nature* **2017**, *541*, 376.
[44] H. Timmers, A. Kowligy, A. Lind, F. C. Cruz, N. Nander, M. Silfies, G. Ycas, T. K. Allison, P. G. Schunemann, S. B. Papp, S. A. Diddams, *Optica* **2018**, *5*, 727.
[45] I. C. Benea-Chelmus, F. F. Settembrini, G. Scalari, J. Faist, *Nature* **2019**, *568*, 202.